

FABRICATION OF TWO DIMENSIONAL SILICON PHOTONIC CRYSTAL

by

SIN YEW KEONG

**Thesis submitted in fulfilment of the requirements
for the degree of
Doctor of Philosophy**

MARCH 2010

ACKNOWLEDGEMENTS

I would like to express my deep and sincere gratitude to many people who made possible the successful outcome of this research work.

First and foremost, I would like to thank my supervisor Prof. Kamarulazizi Ibrahim for giving me the opportunity and resources to complete my PhD. I sincerely thank for his guidance, support, patient and the given freedom in my research.

I am grateful to Ministry of Science, Technology and Innovation (MOSTI) for providing financial support through National Science Fellowship (NSF) scholarship.

I greatly appreciate the timely help and expert assistance from the staff in Nano-Optoelectronics Research and Technology Laboratory (N.O.R. Lab) especially Ee Bee Choo in carrying out measurements on the samples.

I would like to thank Universiti Sains Malaysia for providing the facilities at N.O.R. Lab in School of Physics. I would also like to thank my friends and my colleagues for their moral support.

Last but not least I would like to thank my parents, Sin Song Sang and Wong Lan Ngoh, not only for offering me the shelter of a loving family, but also for fostering my intellectual curiosity throughout the years, for the education they provided me with and for laying the groundwork that ultimately led me to where I am today.

TABLE OF CONTENTS

	Page
ACKNOWLEDGEMENTS	ii
TABLE OF CONTENTS	iii
LIST OF TABLES	vi
LIST OF FIGURES	vii
LIST OF SYMBOLS	xiii
LIST OF ABBREVIATIONS	xv
LIST OF APPENDICES	xvii
ABSTRAK	xviii
ABSTRACT	xx
CHAPTER ONE : INTRODUCTION	
1.0 Introduction	1
1.1 Research Motivations	1
1.2 Research Objectives	5
1.3 Outline of Thesis	5
1.4 Summary	7
CHAPTER TWO : LITERATURE REVIEWS	
2.0 Introduction	8
2.1 Developments of PhCs	8
2.2 Applications of PhCs	17
2.3 Fabrication Techniques	27
2.3.1 Microfabrication method	27
2.3.2 Colloidal crystallization method	34
2.4 Summary	36

CHAPTER THREE : THEORY

3.0	Introduction	37
3.1	Overview of PhCs	37
3.2	PBG Computation	41
3.3	Summary	47

CHAPTER FOUR : PROCESSES AND INSTRUMENTATIONS

4.0	Introduction	48
4.1	Cleaning	48
4.2	Oxidation	49
4.3	Spin Coating	51
4.4	EBL	53
4.4.1	Commercial SEM Conversion System	54
4.4.1 (a)	JEOL JSM-6460LV SEM	56
4.4.1 (b)	Raith ELPHY Quantum Pattern Generator	58
4.4.2	Electron-Solid Interactions and Proximity Effect	60
4.4.3	Electron Beam Resist: PMMA	65
4.5	Wet and Dry Etching	67
4.5.1	BHF and KOH	69
4.5.2	RIE	72
4.6	Characterizations	76
4.6.1	Thickness Determination	76
4.6.1 (a)	Ellipsometer model L116S	77
4.6.1 (b)	Filmetrics F20	80
4.6.2	Surface and Topography Observation: AFM	82
4.7	Simulations Tool: MPB Package	85
4.8	Summary	89

CHAPTER FIVE : EXPERIMENTAL METHODS

5.0	Introduction	90
5.1	Preliminary Works: Optimizations of Parameters in EBL	90
5.2	Step-By-Step Procedures to Fabricate PhCs	93
5.3	Structural Color Effect of PhCs	96
5.4	Summary	98

CHAPTER SIX : RESULTS AND DISCUSSIONS

6.0	Introduction	99
6.1	The Relations of Parameters in EBL	99
6.2	Surface Characterizations in Fabrication Process	110
6.3	Structural Color Effect of PhCs	122
6.4	Summary	123

CHAPTER SEVEN : CONCLUSION AND FURTHER STUDY

7.1	Conclusion	126
7.2	Future Study	128

BIBLIOGRAPHY	130
---------------------	-----

APPENDICES

Appendix A Proof of Bloch's Theorem	138
Appendix B Definition of 'Contrast' and 'Sensitivity' in Resists	140
Appendix C MPB Package	141
Appendix D Raw Data Measured with SEM	148

LIST OF PUBLICATIONS	176
-----------------------------	-----

LIST OF TABLES

		Page
Table 4.1	A list of steps size in pixel and μm for corresponding writefield size that is calculated using Equation (4.3).	60
Table 4.2	Commonly used developers with their composition of MIBK to IPA and their recommended usage.	66
Table 6.1	Combination of parameters for the written lines structure.	100
Table 6.2	A series of electron beam dosage, in $\mu\text{C}/\text{cm}^2$, for different parameters.	108
Table 6.3	Packing factor of the design pattern.	108
Table 6.4	Description of the treatment on (100)-oriented silicon sample wafer and average values of etch depths collected from etching profiles generated by AFM.	113
Table 6.5	List of fabricated PhCs with their PBG.	120
Table 6.6	Summary of the structures fabricated by KOH and RIE etching.	121
Table 6.7	Calculated PBG of the structures fabricated by KOH and RIE etching.	122
Table 6.8	Reflectance spectrums of fabricated 2D silicon PhC calculated with general grating equation.	123
Table 6.9	Reflectance spectrums taken from fabricated 2D silicon PhC and bulk silicon with digital camera at different angles of reflection, θ_r .	124

LIST OF FIGURES

		Page
Figure 1.1	A "photonic micropolis".	2
Figure 2.1	Construction of Yablonovite structure.	11
Figure 2.2	2D PhCs structures with cylindrical (a) deep holes, (b) holes in slab and (c) pillars.	12
Figure 2.3	Construction of a PhC with woodpile structure.	13
Figure 2.4	3D PhCs structures of (a) colloidal structure and (b) inverse opals structure.	14
Figure 2.5	Arrangement for the measurement of PhC optical properties.	15
Figure 2.6	Schematic diagram of the specular ellipsometric measurement setup for the PhC structure.	16
Figure 2.7	Experimental setup of the scanning near field optical microscope.	16
Figure 2.8	(a) Schematic view of a PBG crystal cavity laser structure, and (b) $L-I$ characteristics of a PhC cavity laser and a conventional surface emitting laser.	17
Figure 2.9	SEM images of a fabricated (a) single PhC cavity laser and (b) a coupled PhC cavity array laser.	18
Figure 2.10	Measured photoluminescence spectrum of the coupled cavity array laser.	19
Figure 2.11	(a) SEM image, (b) schematic view of the vertical layer structure and (c) $L-I$ characteristic for PhC-LED device.	20
Figure 2.12	2D PhCs waveguide consisting of (a) a row of missing pores, (b) a row of pores with smaller diameter, (c) coupled-cavity-waveguide and (d) three pore-rows wide of missing pores.	21
Figure 2.13	Measured transmission spectra as a function of wavelength for (a) PhC structures and (b) line-defect waveguides.	22

Figure 2.14	(a) Schematic of waveguide with 90° bend. Electric field pattern at the (b) lower layer and (c) upper layer of the waveguide. (d) SEM image of waveguide with 90° bend.	23
Figure 2.15	SEM images of PCF structures. (a) The solid glass core. (b) Detail of a low-loss solid-core PCF. (c) First hollow-core PCF. (d) PCF extruded from Schott SF ₆ glass.	24
Figure 2.16	(a) 2D PhC slab structures model. (b) Calculated photon flux emitted by two isolated defects.	25
Figure 2.17	SEM image of the fabricated 2D PhC slab structures.	26
Figure 2.18	(a) Top view of the sample observed by optical microscope. (b) Experimental results of trapping and emission of photons by two isolated defects.	26
Figure 2.19	Fabrication processes of 2D PhCs via microfabrication method.	28
Figure 2.20	(a) Cross-sectional SEM-micrograph of a PMMA PhC line defect resonator and (b) SEM-micrograph of a SU8-2000 PhC waveguide.	29
Figure 2.21	Fabrication processes of 3D PhCs via layer-by-layer lithography method.	31
Figure 2.22	The resultant 3D PhC structure fabricated with layer-by-layer method.	31
Figure 2.23	Fabrication processes of 3D PhCs via wafer fusion method.	32
Figure 2.24	Concept of the autocloning method.	33
Figure 2.25	General synthesis schemes for periodic macroporous solids.	35
Figure 3.1	Schematic illustrations of (a) 1D; (b) 2D; and (c) 3D PhCs.	38
Figure 3.2	Superprism phenomena in wavelength sensitive propagation. Light propagates in (a) a PhC and (b) a conventional silicon crystal.	40
Figure 3.3	Superprism phenomena in angle sensitive propagation.	40
Figure 3.4	(a) A diamond lattice of dielectric spheres in air, (b) the reciprocal lattice and (c) the Brillouin zones.	46

Figure 3.5	A photonic band structure.	47
Figure 4.1	(a) Image and (b) cross section of a horizontal tube furnace.	50
Figure 4.2	Static spin processes.	52
Figure 4.3	Example of resist coverage.	52
Figure 4.4	Block diagram shows the major components of a typical EBL system.	55
Figure 4.5	Image of a commercial SEM conversion system.	55
Figure 4.6	A tungsten wire used in SEM.	56
Figure 4.7	(a) Regions and (b) subregions in vector scanning process. (c) The primitive structure is filled by rastering the spot of electron beam.	58
Figure 4.8	Resist profile caused by forward scattering after development (i) positive slope, (ii) vertical, and (iii) negative profile.	61
Figure 4.9	Simulation of electron scattering using CASINO.	63
Figure 4.10	The spin speed versus PMMA film thickness curves.	66
Figure 4.11	Optical properties of 950K molecular weight PMMA resists.	67
Figure 4.12	Etch profiles for (a) purely isotropic, (b) anisotropic and (c) completely anisotropic etching.	69
Figure 4.13	Anisotropic etching on (a) $\langle 100 \rangle$ and (b) $\langle 110 \rangle$ surface.	71
Figure 4.14	(a) Image of a RIE system; and (b) the basic concept of RIE process.	73
Figure 4.15	Proposed mechanism of fluorine-based etching of silicon: (I) formation of released or bonded SiF_2 ; (II) number of bond for the bonded silicon atom reduced; (III) formation of SiF_4 and released.	75
Figure 4.16	Image of ellipsometer.	77
Figure 4.17	Reflection of polarized incident light for ellipsometry.	78

Figure 4.18	(a) Image and (b) setup configuration of Filmetrics F20 thin film measurement system.	80
Figure 4.19	Position of cantilever when the tip measures (a) lower and (b) higher surfaces with contact mode.	82
Figure 4.20	Interaction between probing tip and sample surface in non-contact mode.	84
Figure 4.21	Schematic diagram of the AFM design.	85
Figure 4.22	A simulation example to compute a simple band structure for PhCs.	86
Figure 4.23	The irreducible Brillouin zone of a square lattice.	87
Figure 5.1	(a) The designed lines structure. (b) The dimensions of vertical lines structure.	92
Figure 5.2	The designed 2D PhC structures in (a) square lattice and (b) triangular lattice.	95
Figure 5.3	Experimental setup for observation of structural color.	97
Figure 6.1	Scanning electron micrograph of lines structure written with combination of parameters L1 and beam dosage at (a) $75.0\mu\text{C}/\text{cm}^2$ and (b) $85.0\mu\text{C}/\text{cm}^2$.	101
Figure 6.2	Scanning electron micrograph of lines structure written with combination of parameters L2 and beam dosage at (a) $75.0\mu\text{C}/\text{cm}^2$ and (b) $85.0\mu\text{C}/\text{cm}^2$.	101
Figure 6.3	Scanning electron micrograph of lines structure written with combination of parameters L3 and beam dosage at (a) $75.0\mu\text{C}/\text{cm}^2$ and (b) $85.0\mu\text{C}/\text{cm}^2$.	101
Figure 6.4	Scanning electron micrograph of lines structure written with combination of parameters L4 and beam dosage at (a) $112.5\mu\text{C}/\text{cm}^2$ and (b) $127.5\mu\text{C}/\text{cm}^2$.	102
Figure 6.5	Scanning electron micrograph of lines structure written with combination of parameters L5 and beam dosage at (a) $112.5\mu\text{C}/\text{cm}^2$ and (b) $127.5\mu\text{C}/\text{cm}^2$.	102
Figure 6.6	Scanning electron micrograph of lines structure written with combination of parameters L6 and beam dosage at (a) $112.5\mu\text{C}/\text{cm}^2$ and (b) $127.5\mu\text{C}/\text{cm}^2$.	102

Figure 6.7	Scanning electron micrograph of lines structure written with combination of parameters L7 and beam dosage at (a) $225.0\mu\text{C}/\text{cm}^2$ and (b) $255.0\mu\text{C}/\text{cm}^2$.	103
Figure 6.8	Scanning electron micrograph of lines structure written with combination of parameters L8 and beam dosage at (a) $225.0\mu\text{C}/\text{cm}^2$ and (b) $255.0\mu\text{C}/\text{cm}^2$.	103
Figure 6.9	Scanning electron micrograph of lines structure written with combination of parameters L9 and beam dosage at (a) $225.0\mu\text{C}/\text{cm}^2$ and (b) $255.0\mu\text{C}/\text{cm}^2$.	103
Figure 6.10	Average values of measured line-widths as a function of electron beam dosage for a range of distances between lines.	105
Figure 6.11	Average values of measured line-widths as a function of electron beam dosage for a range of distances between lines.	105
Figure 6.12	Average values of measured line-widths as a function of electron beam dosage for a range of distances between lines.	106
Figure 6.13	An example of designed line structures.	106
Figure 6.14	Electron beam dosage as a function of packing factor for different beam voltages with beam current at (a) 50pA, (b) 75pA and (c) 100pA.	109
Figure 6.15	Scanning electron micrograph of 2D PhC structure on PMMA layer with magnification (a) $2500\times$ and (b) $20000\times$.	111
Figure 6.16	Scanning electron micrograph of 2D PhC structure on oxide layer with magnification (a) $2500\times$ and (b) $20000\times$.	111
Figure 6.17	Scanning electron micrograph of 2D PhC structure on (111)-oriented silicon wafer with magnification (a) $2500\times$ and (b) $20000\times$.	111
Figure 6.18	Corresponding measurement of the structure in Figure 6.15(b).	112
Figure 6.19	Corresponding measurement of the structure in Figure 6.16(b).	112

Figure 6.20	Corresponding measurement of the structure in Figure 6.17(b).	112
Figure 6.21	(a) Scanning electron micrograph of sample (100)-oriented silicon wafer A1, (b) surface topography image and (c) etching profiles from AFM.	114
Figure 6.22	(a) Scanning electron micrograph of sample (100)-oriented silicon wafer A2, (b) surface topography image and (c) etching profiles from AFM.	115
Figure 6.23	(a) Scanning electron micrograph of sample (100)-oriented silicon wafer A3, (b) surface topography image and (c) etching profiles from AFM.	115
Figure 6.24	(a) Scanning electron micrograph of sample (100)-oriented silicon wafer B, (b) surface topography image and (c) an example of etching profiles generated from AFM.	116
Figure 6.25	Scanning electron micrographs of PhCs slab on the silicon wafer of (100)-orientation with magnification (a) 10000 \times and (b) 30000 \times .	117
Figure 6.26	Cross-section images of PhCs slab on the silicon wafer of (100)-orientation with magnification (a) 10000 \times and (b) 30000 \times .	117
Figure 6.27	Photonic band structure of fabricated 2D PhCs slab.	119
Figure 6.28	Proposed 2D PhC structures by etching 1D gratings through Bragg mirrors.	120
Figure 6.29	Scanning electron micrograph of 2D silicon PhC used for observation of structural color effects.	123

LIST OF SYMBOLS

A	pixel area
B	magnetic induction
D	electric displacement
D	beam dosage
$D(\omega)$	density of states of the radiation field in the volume of free space
D_{Si}	thickness of silicon wall
E	electric field
E_R	electric field amplitude of the reflected light
E_I	electric field amplitude of the incident light
G	reciprocal lattice vectors of the photonic crystals
H	magnetic field
I	beam current
J	currents
R_t	resist thickness
V	the volume of free space
V_b	beam voltage
a	lattice constant of photonic crystals
a_i	elementary lattice vectors of the photonic crystals
b_j	elementary reciprocal lattice vectors of the photonic crystals
c	light velocity in free space
d	diameter of pores
d	film thickness
d_f	effective beam diameter due to forward scattering
d_m	dimension of air holes
i	integer
k	wave vector
k_l	extinction coefficient
l_j	arbitrary integers
m	order of the various principal maxima
n	refractive index

n_0	refractive index of air
n_1	refractive index
r	radius of air holes
r_p	reflection coefficient for p -component
r_s	reflection coefficient for s -component
s	deflection speed
t	time
$u_{kn}(r)$	periodic vectorial function
δ_{ij}	Kronecker's delta
ϵ_0	dielectric constant of free space
$\epsilon(r)$	relative dielectric constant of the photonic crystal
κ	Fourier coefficient
λ	reflected wavelength
λ_0	wavelength
μ_0	magnetic permeability of free space
$v_{kn}(r)$	periodic vectorial function
ν	frequency
ω	eigen-angular frequency
ρ	free charges
ρ	complex amplitude reflection ratio
θ_r	angle of reflection
θ_m	angle of incidence
ϕ_0	angle of incidence in ellipsometry

LIST OF ABBREVIATIONS

1D	One Dimensional
2D	Two Dimensional
3D	Three Dimensional
AFM	Atomic Force Microscope
BHF	Buffered Hydrofluoric
CVD	Chemical Vapor Deposition
DAC	Digital-to-Analog Converter
EBL	Electron Beam Lithography
fcc	face-centered-cubic
FDTD	Finite Difference Time Domain
H ₂ O	Water
H ₂ O ₂	Hydrogen Peroxide
HCl	Hydrochloric acid
HF	Hydrofluoric acid
HMDS	Hexamethyldisilazane
GaAs	Gallium Arsenide
IC	Integrated Circuit
IPA	Isopropyl Alcohol
KOH	Potassium Hydroxide
LED	Light-Emitting Diode
LD	Laser Diode
MIBK	Methyl Isobutyl Ketone
MIT	Massachusetts Institute of Technology
MKS	Meter-Kilogram-Second system
MPB	MIT Photonic-Bands
NH ₃	Ammonia
NH ₄ F	Ammonium Fluoride
NH ₄ OH	Ammonium Hydroxide
PBG	Photonic Bandgap
PhC	Photonic Crystal

PCF	Photonic Crystal Fiber
PMMA	Polymethyl Methacrylate
PS	Polystyrene
PWE	Plane-Wave Expansion
QW	Quantum Well
RCA	Radio Cooperation of America
RF	Radio Frequency
RIE	Reactive Ion Etching
SEM	Scanning Electron Microscope
SF ₆	Sulfur Hexafluoride
SiF ₂	Silicon Difluoride
SiF ₄	Silicon Tetrafluoride
SiO ₂	Silicon Dioxide
S-matrix	Scattering matrix
TE	Transverse Electric
TEOS	Tetraethylorthosilicate
TM	Transverse Magnetic
T-matrix	Transfer matrix

LIST OF APPENDICES

	Page
A Proof of Bloch's Theorem	138
B Definition of 'Contrast' and 'Sensitivity' in Resists	140
C MPB Package	141
D Raw Data Measured with SEM	148

FABRIKASI HABLUR FOTONIK SILIKON DUA-DIMENSI

ABSTRAK

Hablur fotonik merupakan bahan yang mempunyai indeks biasan dalam susunan berkala. Apabila gelombang elektromagnetik yang mempunyai julat frekuensi yang lebar merambat melalui bahan tersebut, julat frekuensi tertentu akan terhalang. Frekuensi yang terhalang ini dikenali sebagai jurang jalur fotonik. Dalam kajian ini, satu hablur fotonik silikon dua-dimensi dihasilkan dengan cara mikrofabrikasi. Litografi alur elektron dan proses punaran adalah proses yang penting dalam cara ini. Oleh itu, kerja mengoptimumkan parameter-parameter dalam litografi alur elektron adalah diperlukan. Hubungan di antara parameter-parameter tersebut seperti voltan alur, arus alur, dos alur dan faktor kepadatan dikaji untuk memastikan proses litografi adalah lancar. Seterusnya, pelbagai jenis proses punaran digunakan untuk menghasilkan struktur hablur fotonik dua-dimensi ke dalam wafer silikon. Mikroskop imbasan elektron adalah peralatan kawalan bagi seluruh proses dengan menjalankan pencirian permukaan ke atas setiap struktur yang dihasilkan. Jurang jalur fotonik dihitung dengan perisian "MIT Photonic-bands package" dan kesan warna kestrukturkan diperhatikan dengan susunan alat yang mudah. Daripada keputusan bagi mengoptimumkan parameter-parameter dalam litografi alur elektron, hubungan didapati bahawa dos alur yang tinggi diperlukan apabila arus alur dan voltan alur yang tinggi digunakan; atau struktur yang mempunyai faktor kepadatan rendah dihasilkan semasa litografi alur elektron. Dengan 30kV sebagai voltan alur elektron dan 75pA sebagai arus alur elektron, dos alur elektron bagi mendedahkan struktur dengan 0.65 sebagai faktor kepadatan adalah $177\mu\text{C}/\text{cm}^2$. Dedahan berlebihan berlaku apabila dos alur elektron lebih tinggi daripada nilai ini digunakan

untuk kombinasi parameter ini. Semasa fabrikasi, punaran ion reaktif didapati merupakan peralatan yang sesuai digunakan untuk punaran. Akhir sekali, struktur hablur fotonik dua-dimensi telah berjaya difabrikasikan ke atas wafer silikon jenis-n dengan orientasi-(100). Jurang jalur fotonik bagi hablur fotonik ini yang dihitung adalah dalam julat 2.08-2.73 μm .

FABRICATION OF TWO DIMENSIONAL SILICON PHOTONIC CRYSTAL

ABSTRACT

Photonic crystals are materials with a periodicity in refractive index. When electromagnetic waves with a wide range of frequencies propagate through these materials, certain range of frequencies is prohibited. The prohibited frequencies are known as photonic bandgap. In this study, a two dimensional silicon photonic crystal is fabricated by microfabrication method. Electron beam lithography and etching process are important processes in this method. Hence, preliminary works on optimization parameters in electron beam lithography are necessary. The relations between parameters like beam voltage, beam current, beam dosage and packing factor are studied to ensure lithography process works properly. Subsequently, various types of etching process are applied to create two dimensional photonic crystals structure into a silicon wafer. Scanning electron microscope is the monitoring tool for the whole process by running surface characterization on each fabricated structure. Photonic bandgap is calculated by MIT Photonic-bands package software and the structural color effect of photonic crystal is observed with a simple setup. From the result of preliminary works, the relations of parameters are higher beam dosage is required when higher beam current and higher beam voltage are applied, or a low packing factor structure is exposed during electron beam lithography. With 30kV as electron beam voltage and 75pA as electron beam current, electron beam dosage for exposing the structure with 0.65 as packing factor was $177\mu\text{C}/\text{cm}^2$. Overexposure occurred when electron beam dosage higher than this value was applied for this combination of parameters. During fabrication, reactive ion etching is the appropriate tools for etching. Finally, a two dimensional photonic

crystal structure is successfully fabricated on an n-type silicon wafer with (100)-orientation. The calculated photonic bandgap of this photonic crystal is in the range 2.08-2.73 μm .

CHAPTER 1

INTRODUCTION

1.0 Introduction

First part in this chapter is an overview that casts light on the motivations for this work. Secondly, objectives are listed and a brief orientation to achieve each objective is given respectively. Lastly, a summarize introduction will be presented for each upcoming chapter in this thesis.

1.1 Research Motivations

Since semiconductor been introduced to the field of electronics in the late 1940s, microelectronics industry has developed dramatically. Nowadays microelectronic circuits are keen to our daily lives in almost every aspect. They can be found in commonplace items, such as personal computers, automobiles, household appliances, video and audio entertainment systems; even in toys and digital watches. Miniaturized microelectronic circuits with high-speed performance will always be the target of electronics industry. (Considine and Kulik, 2002) Hence numerous studies had been carried out continuously to achieve this target. Likewise, the invention of semiconductor laser in 1960s accelerated the growth of photonics industry. (Hall et al., 1962) This invention had inspired the scientists turning to photons (or light particles) instead of electrons as the information carrier. This is because the traveling speeds and information capacity of photons in dielectric materials are greater and larger than electrons in metals. Furthermore, photons help in reduction of energy losses because photons are not as strongly interacting as electrons. Hence, optical fiber cables are preferred in recent communications use rather than metallic cables.

Development of optical fiber communication systems has stimulated the creation of various photonic devices. Traditionally, the manipulation of photons relies on the mechanism of total internal reflection. Light propagating in a high-dielectric material is reflected at the interface with a low-dielectric material. The interface between high- and low-dielectric materials must be smooth with respect to the wavelength of light, and this requisite has severely constrained the miniaturization of photonic devices. 20 years ago, a novel class of optical materials known as photonic crystals (PhCs) was proposed with a completely different mechanism for the control of light. PhCs are materials with a periodicity in refractive index. The flow of light in PhCs is molded in same phenomena as the semiconductor does for electrons – a bandgap. When electromagnetic waves with a wide range of frequencies propagate through these optical materials, a small range of frequencies will be prohibited. These forbidden frequencies are known as photonic

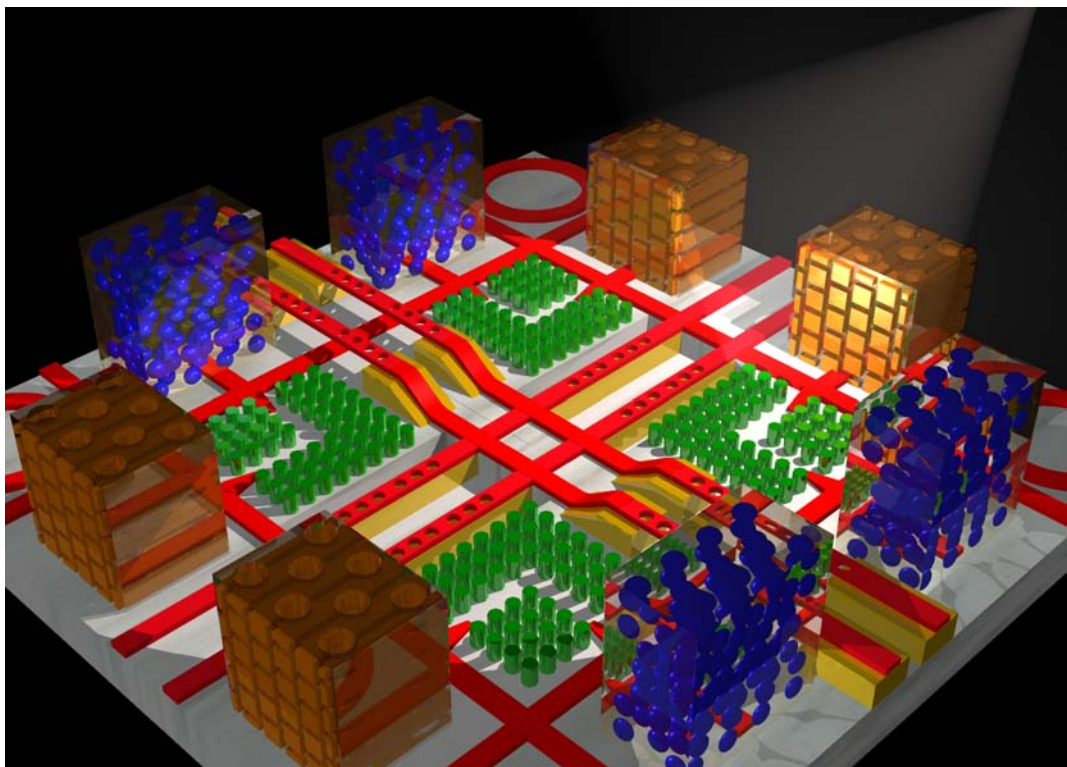


Figure 1.1 A "photonic micropolis" (Johnson and Joannopoulos, 1999).

bandgap (PBG). Hence, scientists start visualizing the assembly of photonic integrated circuits, indeed an optical computer too, from photonic transistors. Figure 1.1 shows a rather fanciful collage of many different PhC devices known as “photonic micropolis” (Joannopoulos, Villeneuve and Fan, 1997).

Enormous number of researches about PhCs was carried out in the last 20 years not only for its interesting properties that may create a photonic transistor, but also due to the application of PhCs promises better performance in photonic devices, for instance, laser diodes (LDs) and light-emitting diodes (LEDs), waveguides, optical fibers, resonators, filters, as well as prisms and polarizers. (Noda and Baba, 2003) In addition, to master the technique in fabricating the crystals structure is also a great challenge. Classification of PhCs is usually depending on their dimensionality, and the fabrication process of the crystals structures is more intricate when the structures dimensionality is increased. Although only three dimensional (3D) PhCs possess a complete PBG, the process to construct a two dimensional (2D) crystal structure is more predictable and controllable. (Birner, 2001) Besides, 2D PhCs are easier to suit in recent photonic devices too. Difficulty in fabricating PhCs is also depending upon the desired wavelength of the bandgap. Since the wavelength of the bandgap scales directly with the lattice constant of the PhCs, optical wavelength PBGs require crystal lattice constant of $<1\mu\text{m}$. Thus state-of-the-art micro- and nanolithography techniques are needed in the fabrication process, such as electron beam lithography (EBL) and X-ray lithography.

Though silicon is a dominant material in microelectronics industry, it only plays the role as a passive or substrate material in the field of photonics. Most of the semiconductor photonic devices are not made from silicon because silicon possesses ‘indirect electronic bandgap’. However, scientists always look forward the chances

to bring silicon into the photonics industry. The discovery of luminescing porous silicon in 1990 (Canham, 1990) and the invention of silicon Raman lasers lately (Ozidal Boyraz and Bahram Jalali, 2004) have convinced the researchers of the possibility of silicon becoming an active optical material. Photon confinement, introduced by building PhCs structure, modifies the optical properties of silicon too. Silicon has high refractive index that allows the fabrication of PhCs with wide PBG because a wide PBG needs a large refractive index contrast. All these properties can be engineered to create a silicon-based integrated photonic circuit. It is believed that fabrication of integrated electronic and photonic circuits on the same silicon wafer could reduce process time, cost and dimensions of the combined chips.

Development of photonic industry is drawing more and more attentions from all over around the world. In the past, the development was hindered by nonexistence of electronic transistor-like photonic devices. However, some scientists recently believe that PhCs, the optical materials that are analogous to semiconductors, are the key to resolve this dilemma. Hence, this work has been carried out to study the fabrication of 2D silicon PhCs and their optical characteristics. Silicon with nanostructure patterns like porous and PhC structures possess optical properties that differ from bulk silicon. This may alter the role of silicon in photonic applications. More silicon-based photonic devices could be produced due to this change; even a silicon-based integrated photonic circuit might be created. As a result, this work also becomes a preparation study for the construction of silicon-based integrated photonic circuits.

1.2 Research Objectives

Several goals have been set at the beginning to ensure this work will be accomplished successfully.

- To optimize EBL technique.
- To develop a suitable etching process in fabricating 2D silicon PhCs.
- To calculate PBG of fabricated PhC.
- To observe the structural color effect of the fabricated PhC.

In this study, a 2D PhC consists of square lattice of air holes in silicon wafer has been successfully fabricated for the first time in Malaysia (Ibrahim and Sin, 2006). By using EBL and reactive ion etching (RIE), the fabricated PhC structure has $807\pm 11\text{nm}$ as the diameter of the air holes, $932\pm 9\text{nm}$ as the periodicity of the air holes and $521\pm 2\text{nm}$ as etch depth of the air holes. The PBG of this PhC structure is in the range $2.08\text{-}2.73\mu\text{m}$ as calculated by MIT Photonic-Bands (MPB) package software.

1.3 Outline of Thesis

This thesis describes the fabrication and characterization of 2D silicon PhCs. Research motivations and objectives of this works are presented as an introduction of this thesis, as well as the thesis's outline.

Chapter 2 provides the history of PhCs. In this chapter, the development of PhCs in methods of fabrication and theoretical methods to calculate PBG are reviewed. Their applications in recent photonic devices are also an important topic covered in this chapter.

A more detailed description on the theory of PhCs is presented in Chapter 3. This chapter describes the physical and experimental background of PhCs. PBG

structure is calculated with plane wave expansion methods involving Maxwell's equations. The methods of fabrication with corresponding materials and structures are also shown in this chapter.

Chapter 4 covers basic concept of several main instruments, systems, materials and techniques used for fabrication and characterization purposes. For fabrication process, EBL and etching are main discussion topics. Meanwhile, physics behind the characterization tools like atomic force microscope (AFM), scanning electron microscope (SEM) and ellipsometers are explained. This chapter will also include an explanation on simulation tool used for the computation of PBG.

In Chapter 5, descriptions of experimental methods in fabricating PhCs and characterizing the fabricated crystals structure are provided. Optimizations of parameters in EBL are preliminary works before fabrication of PhCs. Then, step-by-step procedures to achieve the desired crystal structures are demonstrated. A simple setup to study structural color effect of the fabricated crystal structure is introduced as well.

Chapter 6 shows the resultant crystal structures at each fabrication process steps with discussions. Optimization of EBL is required in our fabrication process. This chapter covers the resultant topography images captured by SEM, calculated bandgap structures with simulation tools and the structural color effect of fabricated structures.

Lastly, this thesis is ended with conclusions of our works in Chapter 7. In addition, some potential future studies are listed and discussed for the interest of people who would like to continue on this topic.

1.4 Summary

Topics covered in this introduction chapter are research motivations, research objectives and outline of this thesis. PhCs, an optical materials analogy to the semiconductors, may play an important role in photonics industry similar to the semiconductor in microelectronics industry. Hence fabrication and characterization of PhCs is a valuable study in recent and future research, especially for the silicon PhCs. The optical properties of silicon could be altered with the assistance of these structures; and this may increase the utilization of silicon in photonic applications. Parameters and settings used in EBL require optimization; and a suitable etching process is developed to ensure silicon PhCs are fabricated successfully. PBG structures are studied theoretically with MPB package software and the structural color effect of the fabricated crystal structure is observed.

CHAPTER 2 LITERATURE REVIEWS

2.0 Introduction

The study and development of PhCs grow rapidly in the last 20 years since their first commenced. In this chapter, we will firstly discuss the development of PhCs on photonic band structure computational methods, the fabricated crystals structures and characterization methods. Then, applications of PhCs in the field of photonic and their achievements will be reviewed. Lastly, two fabrication methods of PhCs are introduced, which are microfabrication method and colloidal crystallization method.

2.1 Development of PhCs

Though the idea of PhCs had surprised the entire photonic society in 1987, this phenomenon actually had been studied 120 years ago. In 1887, the phenomenon of electromagnetic waves propagation in periodic structure was firstly studied by Lord Rayleigh. He stumbled onto a form of the Bloch-Floquet theorem and derived quite a general solution for waves in one dimensional (1D) periodic structure. He identified the fact that they have a narrow bandgap prohibiting light propagation through the structure. This bandgap is angle-dependent. Propagating light at different angles of incidence towards the structure, which experiences different periodicities, reflects different wavelength of light. Unfortunately, he failed to pursue this result into 2D and 3D periodic structures. (Johnson and Joannopoulos, 2001)

It was until year 1987; Yablonovitch (1987) and John (1987) managed to introduce the concept of omnidirectional PBGs in two and three dimensions by marrying solid-state physics and electromagnetism. In their study, Yablonovitch

(1987) proposed the possibility to control the radiative properties of materials with the appearance of PBGs; while John (1987) proposed the occurrences of photon localization when randomness was introduced in a uniform PhC structure. John suggested this localization would be due to a similar phenomenon in electronic system known as Anderson localization. However Yablonovitch et al. (1991b) described the localization phenomenon as doping.

Discussions on PBG by Yablonovitch (1987) and John (1987) drove rapidly the development of the methods for analyzing PhCs. Some theoretical researchers of solid state physics strengthened the foundation for PhC analysis by using plane wave expansion (PWE) method (Leung and Liu, 1990; Zhang and Satpathy, 1990; Ho, Chan and Soukoulis, 1990). In this method, a periodic boundary condition is applied on the scalar approximated wave equation to determine an eigenvalue equation. It is an optical version similar to the method used in solid state physics.

At the beginning, the photonic band structure of a face-centered-cubic (fcc) lattice of spheres was calculated because an experimental result of that crystal structure was reported by Yablonovitch and Gmitter (1989). The works of Leung and Liu (1990) as well as Zhang and Satpathy (1990) showed rather good agreement with the reported experimental results, except they failed to find a true gap from their band structure. Leung and Liu (1990) believed spherical atomic symmetry produced a degeneracy between valence and conduction bands at the W point of the Brillouin zone, allowing only pseudogap, rather than a full PBG. Ho, Chan and Soukoulis (1990) were the first to overcome this problem. They had determined that dielectric spheres arranged in the diamond structure do possess a full bandgap. Following this discovery, Yablonovitch, Gmitter and Leung (1991a) introduced an fcc lattices

structure consisting of nonspherical atoms known as Yablonovite. This structure solved the problem of degeneracy and permitted a full PBG in fcc lattice structure.

Up to now, all discussions are considering infinite periodicity in all directions. To calculate band structure of PhCs with some defects, Yablonovitch et al. (1991b) introduced the supercell method. In this method, the plane wave (PWE) method is applied with definition of unit cell as a set of PhC periods around the defect. However, this method takes a long time to calculate the complicated defect structures.

Transfer matrix (T-matrix) method is a combination of finite element analysis and multilayer analysis methods. This method has significant advantages of speed and convenience in calculating the band structure. It was developed by Pendry and MacKinnon (1992) and, for the first time, transmission characteristics of finite periodic structures were analyzed effectively. However, a better computational approach based on T-matrix method called scattering matrix (S-matrix) method was developed to calculate the electromagnetic properties of multilayer dielectric structures with an arbitrary in-plane periodic patterning. While the T-matrix gives the amplitude of both incoming and outgoing waves at the surface in terms of those in the substrate, the S-matrix relates the amplitudes of the outgoing waves at the surface and in the substrate, to those of the incoming waves on either side of the structure. Hence, S-matrix method includes the coupling of the internal electromagnetic modes to external fields, so it provides a straight forward way of calculating reflectivity and emission spectra for patterned waveguide structures (Whittaker and Culshaw, 1999). Actually, the S-matrix method was originated from the context of electron tunneling through multilayer semiconductor structures (Ko and Inkson, 1988).

About the same time, another method, finite difference time domain (FDTD) method, was applied to the computation of photonic band structure (Mekis et al.,

1996; Joannopoulos, Villeneuve and Fan, 1997). FDTD method is a regular numerical tool used to calculate the space and time changes in the electromagnetic fields of light by using a finite difference method. Compare to other previous discussed methods, FDTD method has a higher degree of flexibility in PhCs design structure. Optical properties of 2D structures like PhCs waveguide, crystals structures with point or line defects; as well as 3D structures like colloidal structures were able to be determined by applying FDTD method. Hence, it can be widely used in various application fields in both the research and development areas. However, FDTD method requires large computer memories and long calculation time. Thanks to the remarkable progress in computer technology, this problem has no longer been a serious dilemma anymore.

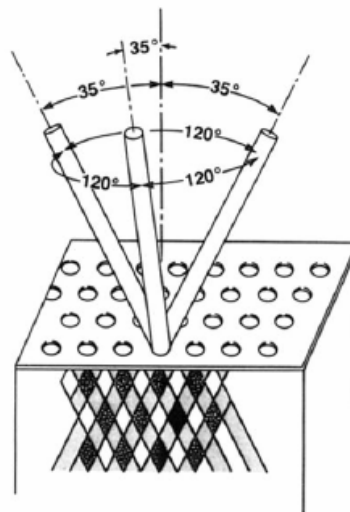


Figure 2.1 Construction of Yablonovite structure (Yablonovitch, Gmitter and Leung, 1991a).

In parallel with these theoretical studies, progress was also made with the experimental challenges of fabrication. Analogy to electronic bandgap of the semiconductors, PBG of the PhCs is also determined by lattice constant, the spatial

period of the stack. At the beginning, PhCs were fabricated by means of mechanical techniques. Hence, only crystals structures with large lattice constant and worked in the microwave and millimeter-wave regions were produced. For instance, a PhC consisting of spherical air atoms was constructed by stacking a series of drilled hemispheres; (Yablonovitch and Gmitter, 1989) as well as an fcc crystal of the Wigner-Seitz cells known as Yablonovite was formed by drilling dielectric material as shown in Figure 2.1. To construction the Yablonovite structure, a slab of dielectric material was first covered by a mask containing triangular array of holes. Then, three drilling operations were conducted through each hole, 35.26° away from normal and spread out 120° on the azimuth by a real drill bit for microwave work (Yablonovitch, Gmitter and Leung, 1991a).

In order to construct a PhC that works in optical frequency regions, state-of-the-art microfabrication techniques are needed in producing lattice constant with the dimension of micrometer and nanometer. In other words, fabrication techniques of PhCs rely on the development of microfabrication processes in microelectronics industry, which include lithography techniques like photolithography and EBL, wet and dry etching technique, as well as thin film deposition methods such as sputtering, evaporative deposition, chemical vapor deposition (CVD) and epitaxy.

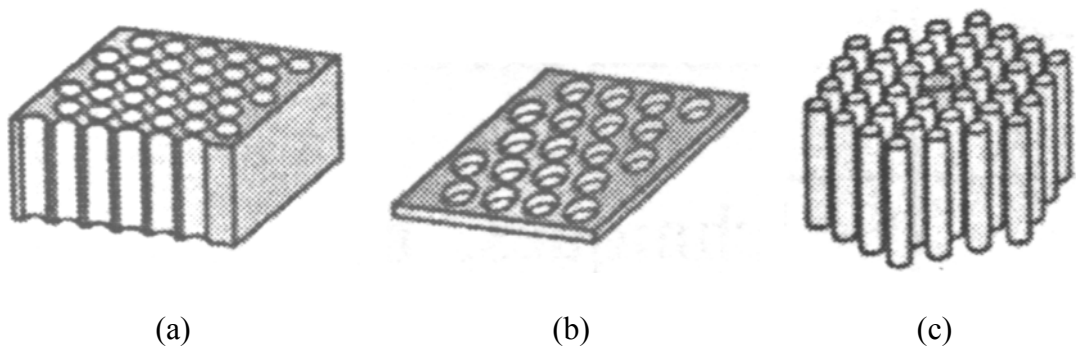


Figure 2.2 2D PhCs structures with cylindrical (a) deep holes, (b) holes in slab and (c) pillars (Hasegawa, 2003).

In 1993, a triangular array of air columns in gallium arsenide (GaAs) was fabricated successfully by performing etching with EBL (Wendt et al., 1993). Since then, the periodically arranged cylindrical holes or pillars in triangular or square structure has become the most commonly fabricated and studied 2D PhCs structure as shown in Figure 2.2. In addition, some researchers attempted to produce a 3D PBG based on that particular structure, such as Fan et al. (1994), as well as Johnson and Joannopoulos (2001). The 2D PhCs structure is also well-fitted in the constructions of photonic devices like LD, LED, waveguide, filter and polarizer.

With the assist of EBL and dry etching, a PhC with woodpile or stacked-stripe structure like Figure 2.3 was fabricated as well. It was formed by stacking layers of semiconductor stripes and possessed a PBG within infrared (10-14.5 μm) and mid-infrared region (5-10 μm) reported by Lin et al. (1998) and Noda et al. (1999) respectively. Following these motivated results, a PBG within near-infrared wavelength range (1.3-1.55 μm) was obtained by shrinking the stripe period, width and thickness of the semiconductor stripes (Noda et al., 2000).

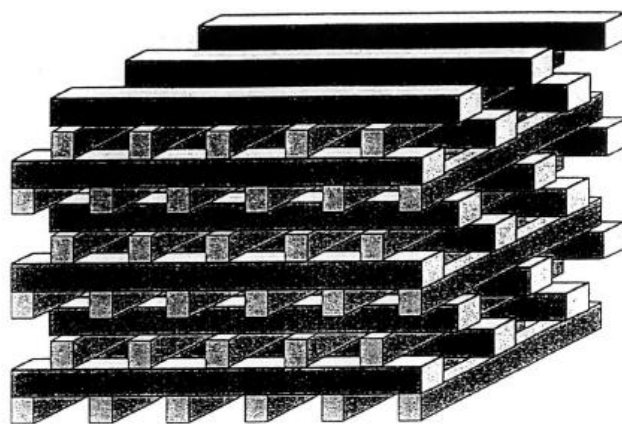


Figure 2.3 Construction of a PhC with woodpile structure (Ho et al., 1994).

Colloidal crystallization processes had been studied for several decades; (Pieranski, 1983) and colloidal structures drew attentions of chemists and physicists once the idea of PBG was introduced in 1987. It is the easiest and cheapest method to achieve a 3D PhCs structure. Nevertheless, by infiltrating the gaps between colloidal structures with semiconductors or polymers, a novel structure known as inverse opals was obtained. In both inverse opals and colloidal structures, PBG are determined by the diameter of spheres. Fukuda et al. (1998) and Subramania et al. (1999) respectively reported PhCs in colloidal structure and inverse opals structure possessed PBG at 502nm and 521nm where diameter of spheres were 220nm and 395nm. Colloidal structure and inverse opals structure are shown in Figure 2.4.

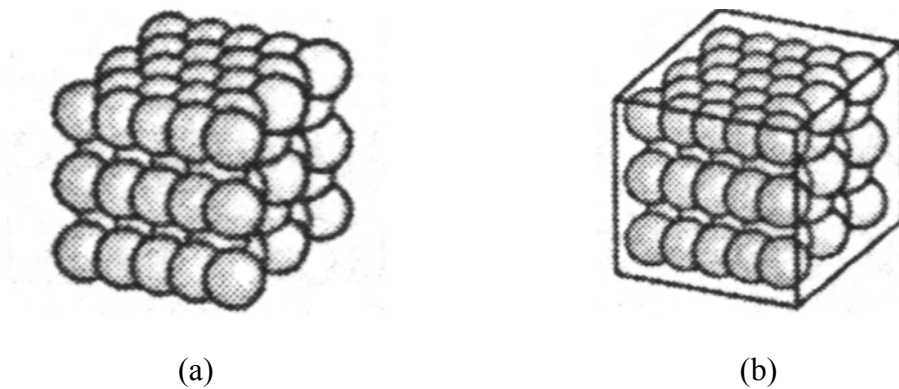


Figure 2.4 3D PhCs structures of (a) colloidal structure and (b) inverse opals structure (Hasegawa, 2003).

There are many other structures and fabrication techniques that have been developed in last 20 years. Autocloning method (Kosaka, 1998), photopolymerization technique (Sun, Matsuo and Misawa, 1999), anodic etching technique (Birner et al., 2001) are few of the examples. In the future, it is believed that many new PhCs structures are going to be proposed due to recent development of microfabrication techniques.

In general, optical transmission and reflection measurements are performed on PhCs structures to study the PBG experimentally. The transmission and reflection spectra can be measured by spectrometer with corresponding wavelengths, including infrared, visible and ultraviolet wavelengths range. For instance, Figure 2.5 shows an arrangement for the measurement of PhC optical properties using the photoluminescence spectrometer. A photoluminescence of quantum well (QW) was embedded in the waveguide as an internal source and light was guided passing through a PhC structures then collected at a cleaved edge. A micro-positioning setup in three dimensions is usually attached within these instruments to ensure the light beam pass through the structures at the direction perpendicular to the periodicity. However, this method face problem in characterizing 2D PhCs slab. Hence, a simple and non-destructive optical characterizing method was carried out by using specular spectroscopic ellipsometry as illustrated in Figure 2.6. Differed from previous method, reflection spectra at different angles of incidence and reflection are collected and studied to calculate the PBG. Both discussed methods to study the far field optical characteristics of PhCs, near field characteristics was proposed once the

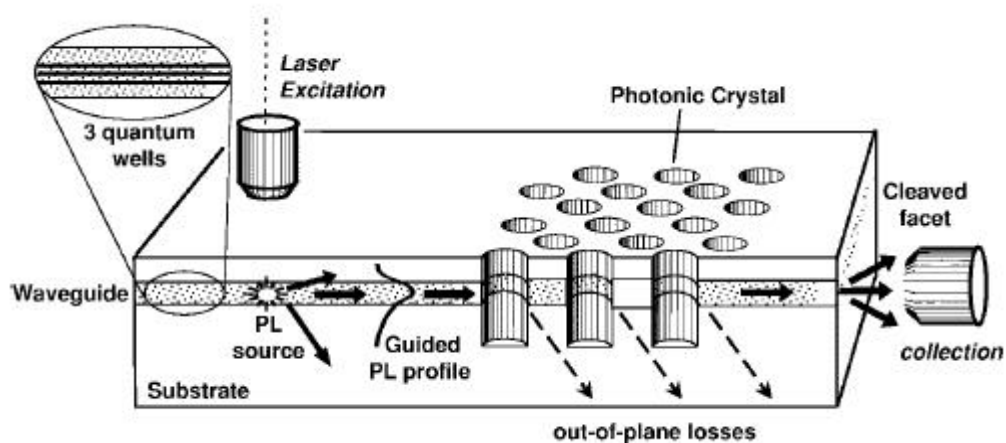


Figure 2.5 Arrangement for the measurement of PhC optical properties (Labilloy et al., 1999).

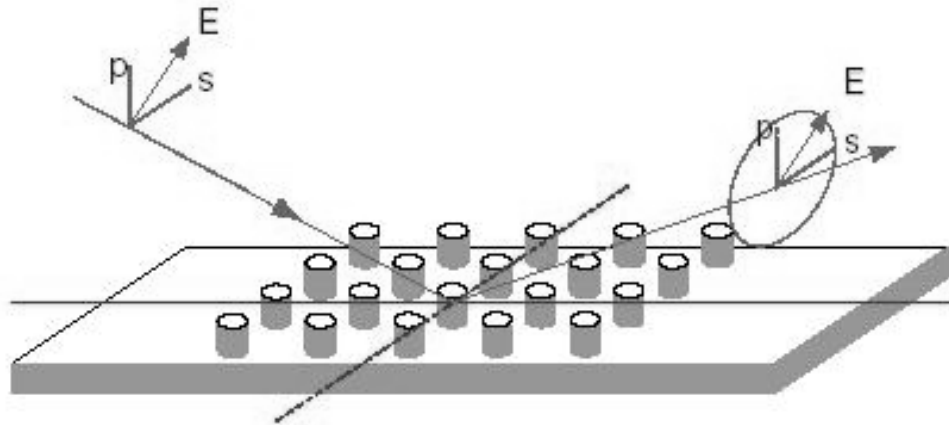


Figure 2.6 Schematic diagram of the specular ellipsometric measurement setup for the PhC structure (Lin et al., 2006).

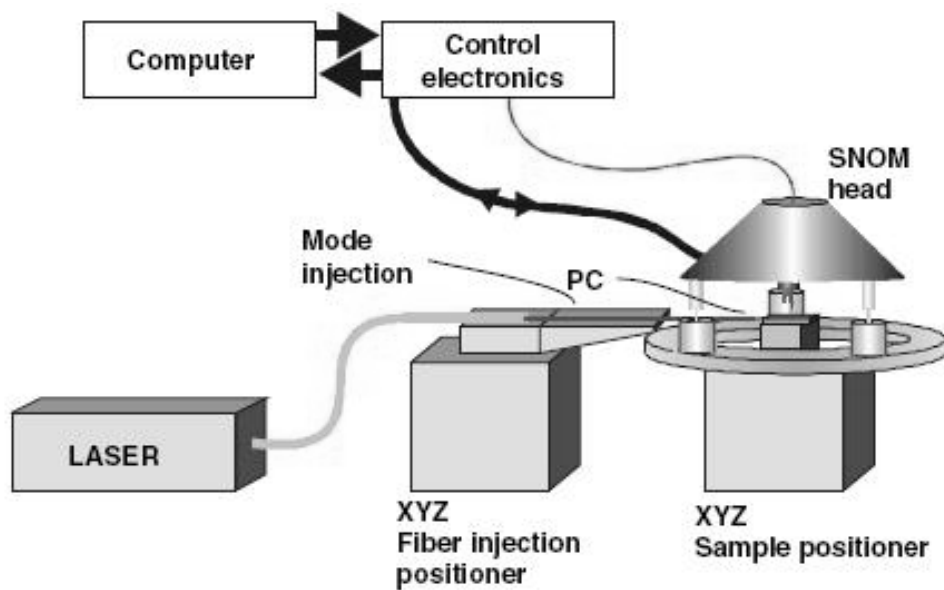


Figure 2.7 Experimental setup of the scanning near field optical microscope (Bernal et al., 2006).

scanning near field optical microscope was introduced. The experimental setup of this method is working in collection mode as shown in Figure 2.7.

Developments of PhCs in PBG computational methods, fabrication techniques and fabricated structures, as well as the characterization methods are

reviewed. A more detailed explanation on each fabrication techniques including their processes will be described later in Section 2.3.

2.2 Applications of PhCs

In previous chapter, it was explained that information carriers are going to be changed from electrons to photons in communications system. It was believed that PhC is the key to stimulate the development of this idea. Hence, novel photonic devices integrated with PhCs structures were proposed from time to time. The involved photonic devices are LD and LED, waveguide, filter and polarizer, as well as optical fiber. Thus, functionality of PhCs also becomes a measure of progress in their development besides the computational models, fabrication techniques and characterization methods. Recently, some theoretical and experimental results prove the crystals structures periodicities promise better performance in those devices.

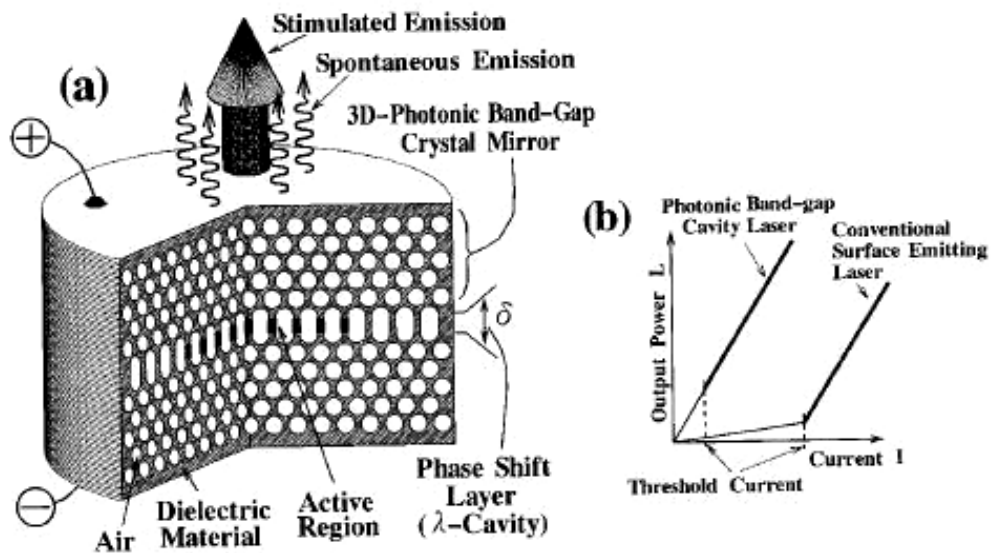


Figure 2.8 (a) Schematic view of a PBG crystal cavity laser structure, and (b) L - I characteristics of a PhC cavity laser and a conventional surface emitting laser (Hirayama, Hamano and Aoyagi, 1996).

Optical resonators are major components of lasers. They are surrounding the active medium region to amplify light waves by reflecting them into the gain region several times. Smooth and parallel-cleaved edges and dielectric mirrors made from alternating high and low refractive index quarter-wave thick multilayer (or known as diffraction Bragg reflector) are commonly found as the optical resonators in LDs. Hirayama, Hamano and Aoyagi (1996) proposed a novel surface emitting laser, consisting of a 3D PBG crystal cavity as shown in Figure 2.8(a). The analysis of PBG with PWE method by using 2D model showed that, this laser operates as a thresholdless (no kink in the $L-I$ curve, contrary to conventional surface emitting lasers, as shown in Figure 2.8(b)), spatial-emission-noiseless, high efficiency and high power light source.

In 2005, Altug and Vučković (2005) experimentally demonstrated a coupled PhC nanocavity array laser. By coupling large numbers of PhC cavities, they believed this laser can achieve comparable output powers to conventional vertical cavity surface emitting laser, but at much lower threshold pump powers. Figure 2.9

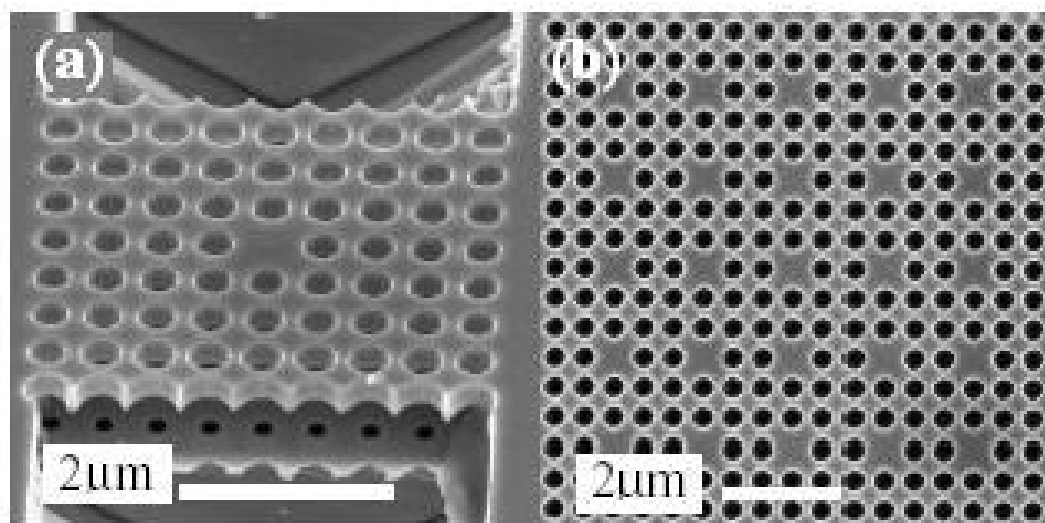


Figure 2.9 SEM images of a fabricated (a) single PhC cavity laser and (b) coupled PhC cavity array laser (Altug and Vučković, 2005).

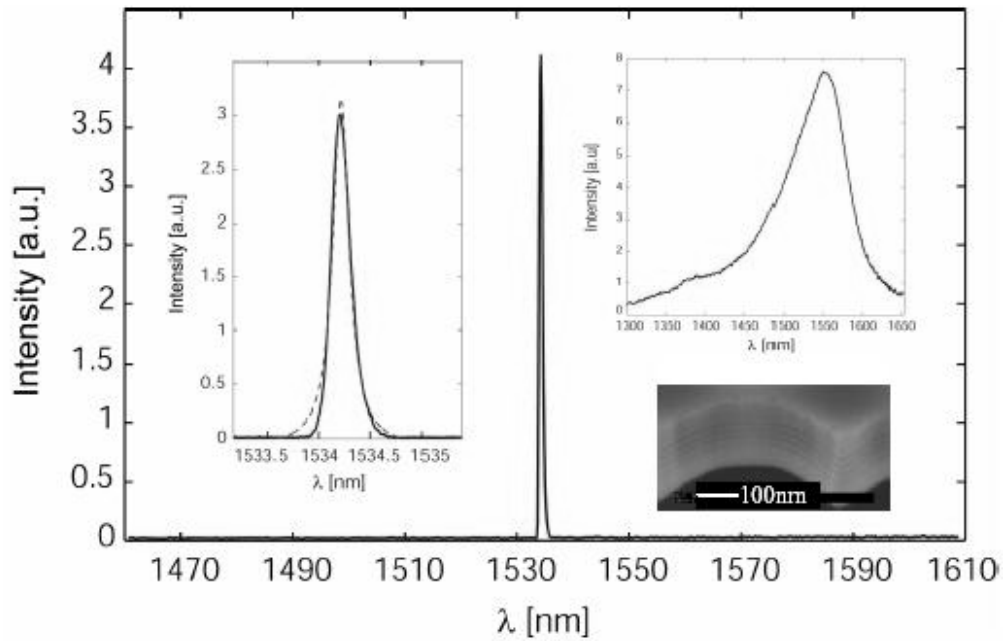


Figure 2.10 Measured photoluminescence spectrum of the coupled cavity array laser (Altug and Vučković, 2005).

shows the SEM image of fabricated PhC cavity array laser. Figure 2.10 shows measured photoluminescence of the coupled cavity array laser with a peak at 1534nm. The PhC hole radius in this structure was about 192nm. The inset on the left in Figure 2.10 shows the zoomed-in portion of the spectrum fitted with a Lorentzian (dashed curve) of 0.23nm linewidth, while the inset on the right shows the QW photoluminescence from unprocessed wafer. QWs were shown on the SEM image.

Similar to LDs, application of PhCs structure in LED devices also improve their performance. Kim et. al (2005) reported a gallium nitride-based LED integrated with square-lattice 2D-PhC structures emitting wavelength around 400nm, as shown in Figures 2.11(a) and (b). Figure 2.11(c) shows the $L-I$ characteristic for PhC-LED chips with lattice constants of 300nm (●), 500nm (■), and 700nm (▲), together with that from a planar reference device (○) for comparison, while the inset is the electroluminescence enhancement factor of PhC-LEDs relative to the reference LED.

The resultant LEDs showed significant improvements in light extraction, up to 2.1 times that of planar LEDs without PhC integration. They concluded this improvement results from the efficient diffraction of light in the surface-normal direction by the integrated 2D-PhC structure.

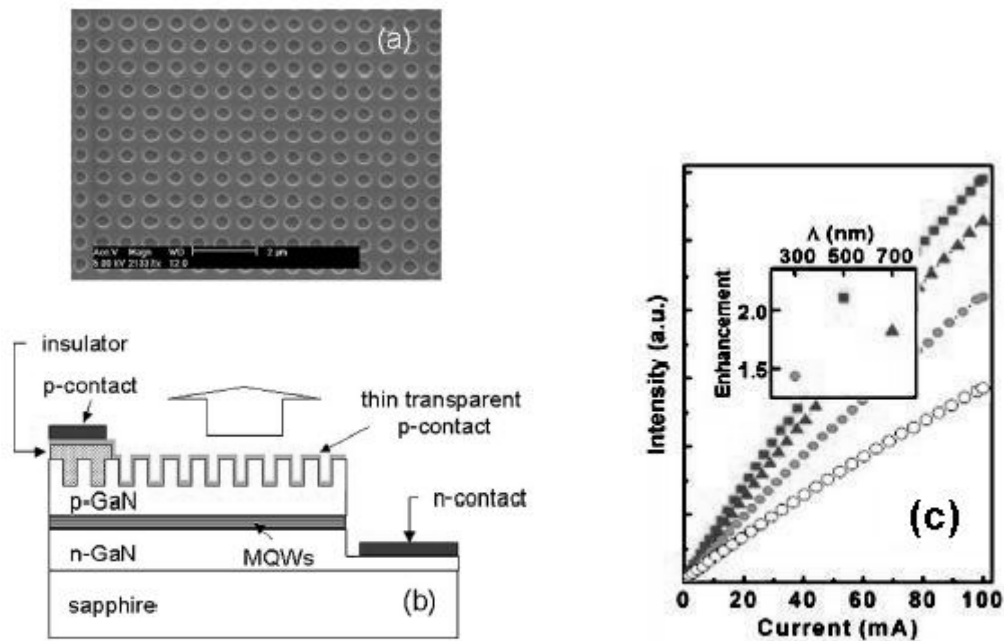


Figure 2.11 (a) SEM image, (b) schematic view of the vertical layer structure and (c) L - I characteristic for PhC-LED device (Kim et al., 2005).

Conventional optical waveguides structure in which a dielectric material with high refractive index is surrounded by a material with lower refractive index, are guiding optical waves based on the principle of total internal reflection. Common types of optical waveguides include slab waveguide and optical fiber. They are used as components in integrated optical circuits or as the transmission medium in local and long haul optical communication systems.

The introduction of PBG into the field of wave guiding creates novel class of slab waveguide and optical fiber. To construct a PhCs-based optical waveguide, a

line defect is introduced into the PhC structure by changing the pore radius of an entire pore line or removing it completely. The forbidden frequencies in bulk PhCs are localized in the surrounding of the defect and this line defect will act as a waveguide. Figure 2.12 lists some examples of waveguides in 2D PhCs (Jamois et al., 2003).

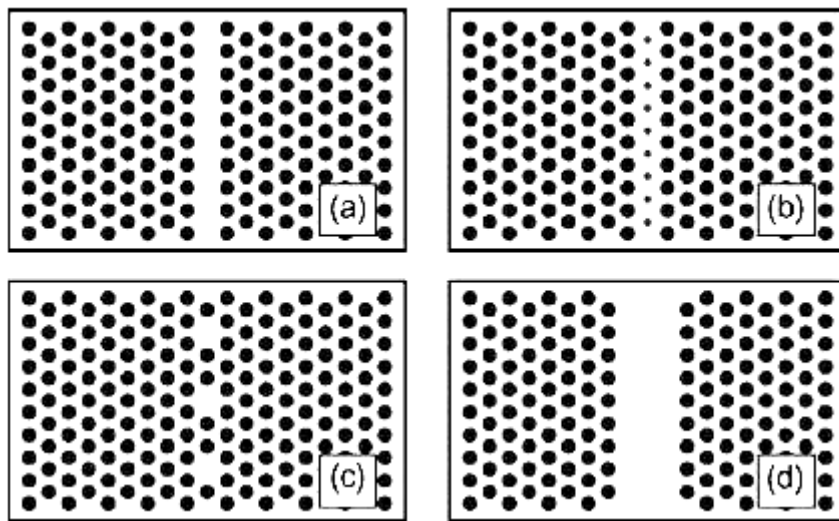


Figure 2.12 2D PhCs waveguides consisting of (a) a row of missing pores, (b) a row of pores with smaller diameter, (c) coupled-cavity-waveguide and (d) three pore-rows wide of missing pores (Jamois et al., 2003).

An experimental work on PhC-based waveguide was carried out by Assefa et al (2004). The fabricated waveguide consisted of GaAs-based dielectric rod arrays, while a row of rods with smaller diameter was introduced into the bulk PhCs. The inset SEM image in Figure 2.13(a) shows a bulk PhC consisted of four rows of GaAs-based rods. The transmission spectra for fabricated bulk PhCs with two and four rows of rods were measured and the creation of a PBG for the wavelength range of 1448-1482nm was observed in the case of four rows of rods, as shown in Figure 2.13(a). Meantime a PhC-based waveguide was formed by introducing a row of

GaAs-based rods with smaller diameter into the bulk PhC as shown in the inset of SEM image in Figure 2.13(b). The measured transmission spectra for two similar PhC-based waveguides (known as Device 1 and Device 2) are shown in Figure 2.13(b). An increase in transmission is observed within the measured bandgap, demonstrating lateral guiding of light due to the PBG rather than total internal reflection (Assefa et al., 2004).

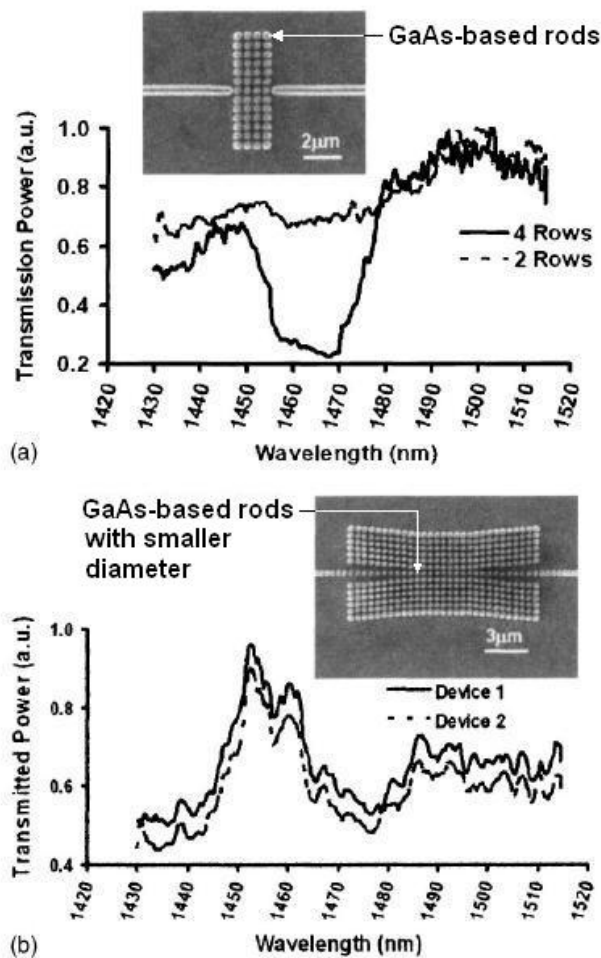


Figure 2.13 Measured transmission spectra as a function of wavelength for (a) PhC structures and (b) line-defect waveguides (Assefa et al., 2004).

Waves guiding in conventional optical waveguides are constrained by critical angle when total internal reflection occurs, but this phenomena does not happen in

PhCs-based waveguide. A 3D PhCs-based waveguide with 90° bend has been demonstrated theoretically and experimentally by crossing two waveguides as shown in Figure 2.14(a). Through 3D FDTD method, the optical transmission behavior of the bend waveguide is calculated and shown in Figure 2.14(b) and (c). Light propagates through the waveguide formed in the lower layer before the bend, then moves to the upper layer when it reaches the bend corner and propagates through the waveguide formed in the upper layer as shown in Figures 2.14(a) (Chutinan and Noda, 1999). An actual 3D PhCs-based waveguide with 90° bend was successfully constructed as shown in Figure 2.14(d) (Noda et al., 2000).

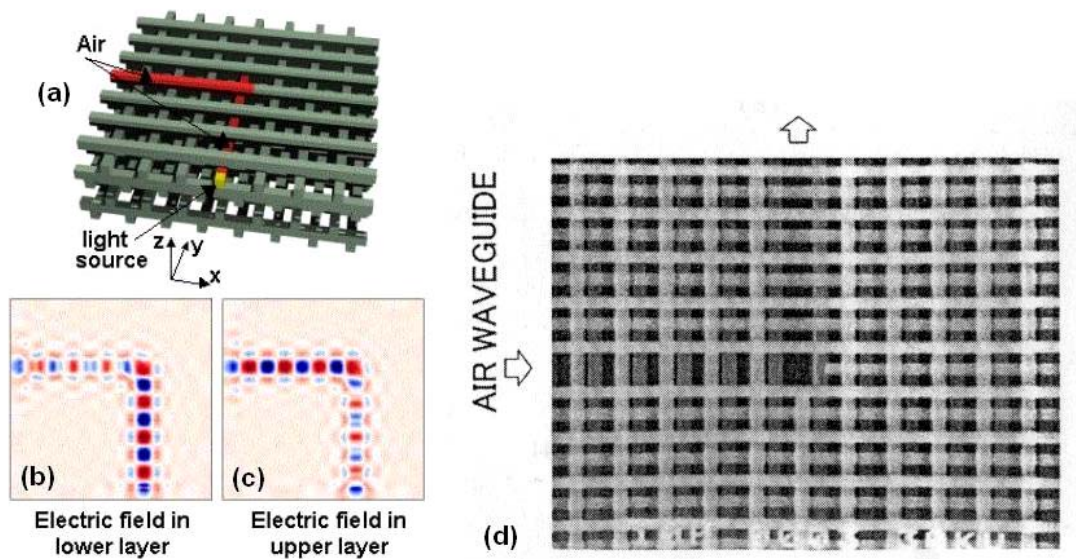


Figure 2.14 (a) Schematic of waveguide with 90° bend. Electric field pattern at the (b) lower layer and (c) upper layer of the waveguide (Chutinan and Noda, 1999). (d) SEM image of waveguide with 90° bend (Noda et al., 2000).

Photonic crystal fiber (PCF), or also called microstructures fiber, is a new class of optical fiber based on the properties of PhCs. Similar to conventional optical fiber; PCF also consisted of a core and a cladding. However, the cladding of PCF is

periodically arranged holes. Some selected SEM images of fabricated PCF structures are shown in Figure 2.15. The first working PCF is a solid glass core as shown in Figure 2.15(a) and (b). A low-loss solid-core PCF is surrounded by a triangular array of 300nm-diameter air channels, spaced 2.3 μm apart (Russell, 2006). PCF is interesting for a number of reasons, not the least of which is its ability to guide light in an air core, for example hollow-core PCF shown in Figure 2.15(c). Guiding light in an air core can definitely avoid both optical absorption and dispersion. Moreover, a much higher intensity of light can be transmitted in an air-core than a glass-core fiber. At the same time, air absorbs less light than glass does, thus a lower thermal load prolongs the life span of air-core fiber (Mannstadt, 2005). Figure 2.15(d) shows a PCF extruded from Schott sulfur hexafluoride (SF_6) glass with a core $\sim 2\mu\text{m}$ in diameter (Russell, 2006).

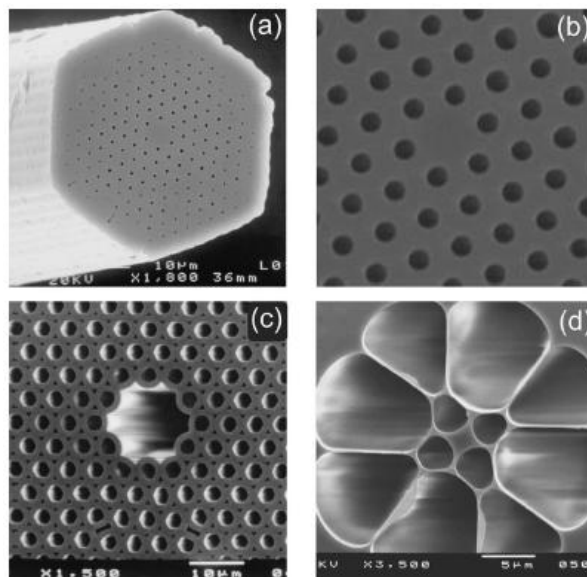


Figure 2.15 SEM images of PCF structures. (a) The solid glass core. (b) Detail of a low-loss solid-core PCF. (c) First hollow-core PCF. (d) PCF extruded from Schott SF_6 glass (Russell, 2006).

A demonstration by Noda, Chutinan and Imada (2000) showed the phenomenon that propagating photons in a line-defect waveguide were trapped by point defects and emitted to the vertical direction. From their observation, the localization phenomenon were applicable in the construction of channel add/drop filtering devices. In their work, a 2D PhC slab structures in a triangular lattice was used as the model for calculation as shown in Figure 2.16(a). The radius of air holes, point defect i and j , as well as slab thickness were designed to be $0.29a$, $0.56a$, $0.58a$ and $0.60a$ respectively with the lattice constant, $a=0.42\mu\text{m}$. Referring to Figure 2.16(b), photons with different frequencies of f_i and f_j were trapped and emitted to free space by the corresponding point defects with the top axis showed the wavelength for $a=0.42\mu\text{m}$. For the experimental result, an indium gallium arsenide phosphorus 2D PhC slab structures surrounded by air in the vertical direction, was fabricated. Referring to Figure 2.17 and 2.18(a), a straight waveguide and isolated defects labeled i and j were formed on the 2D PhC slab structures. The light was injected to the waveguide from the right edge of the slab and observed by infrared camera as shown in Figure 2.18(b). When the input light frequency was tuned at

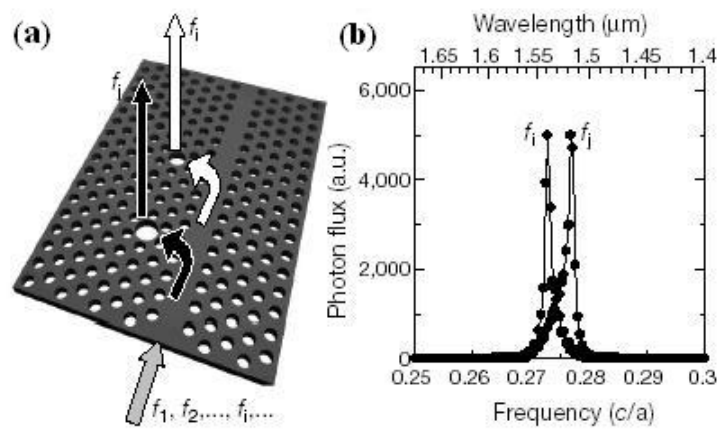


Figure 2.16 (a) 2D PhC slab structures model. (b) Calculated photon flux emitted by two isolated defects (Noda, Chutinan and Imada, 2000).